Asymmetric modal coupling in a passive resonator towards integrated isolators

Jun Wang [●],[1] Qi Liu,[1] Jie Lin,[1,2] Peng Jin,[2,3] Shutian Liu,[1] and Keya Zhou [●][1,*]

[1]*School of Physics, Harbin Institute of Technology, Harbin 150001, China*
[2]*Key Laboratory of Micro-systems and Micro-structures Manufacturing, Harbin Institute of Technology,*
Ministry of Education, Harbin 150080, China
[3]*School of Instrumentation Science and Engineering, Harbin Institute of Technology, Harbin 150001, China*

Asymmetric response is essential to form a nonlinearity-based nonreciprocal device. Here, we studied the asymmetric modal coupling in a passive resonator driven by the nonconservative coupling add-drop filter (NCC-ADF). When light is incident from either port, the proposed configuration can selectively excite supermodes and realize an asymmetric stored optical energy in the passive resonators. Such asymmetry can be tuned on demand by varying the amplitude and phase delay of the mirror system. Furthermore, by introducing the thermal-optic nonlinearity effect in the proposed configuration, an optical isolator with low-power and broadband nonreciprocal optical transmission can be realized. The linear and nonlinear mode dynamics in the NCC-ADF configuration with asymmetric modal couplings were effectively described through a temporal coupled mode theory. The theoretical result will find potential application in on-chip integrated isolators as well as microcavity-based applications.

I. INTRODUCTION

Nonreciprocal components are critical to control optical signal routing, which is important in realizing large-scale and complex photonic integrated circuits (PICs) [1,2]. The central concept of realizing optical nonreciprocity is to break the Lorentz reciprocity theorem [3] through one of the three approaches: magneto-optic effect [4–6], active-driven modulation [7–9], or optical nonlinearity [10–13]. Faraday magneto-optic effect has been widely used in free-space and fiber-based communication systems, yet their on-chip integration has been challenging due to its incompatibility with complementary metal oxide semiconductor (CMOS) fabrication [9]. Approaches based on the active-driven modulation have seen remarkable progress in magnet-free isolators, but the dynamic response of the material is extremely demanding, and the external drive requires additional fabrication and power consumption. Additionally, large amounts of electromagnetic background generated by the high-power radio-frequency drives will interfere with the sensitive electronics and photodetection in photonic integrated circuits [13]. The nonlinearity-based approach is inherently constrained by the limit of dynamic reciprocity to form a real isolator under simultaneous two-port excitations [14]. It also has some general limitations such as the trade-off on input power and spectra width, limited maximum forward transmission, and long pulse duration constraints [10]. However, the approach is still attractive because it requires no external biasing field and drivers [12]. Plenty of effort has been done to bypass or even overcome the above-mentioned limits such as

using the spontaneous chirality [15], nonlinear chirality [16], velocity selective nonlinearity [17], parity-time symmetry [18,19], loss-induced nonreciprocity [20], two-dimensional materials [21], moving photonic crystal [22], and spin resonators [23,24].

Recently, mirror systems have been integrated with a ring resonator to achieve a series of unconventional physical mechanisms and valuable functionalities, including exceptional point enhanced phase sensing [25], sensing with exceptional surfaces combine sensitivity with robustness [26], second-order exceptional point [27], higher-order exceptional point [28], chirality and degenerate perfect absorption [29], optical amplifier [30], on-chip integrated microlaser [31], etc. However, most studies have overlooked the potential impact of reflected light caused by a mirror system on the stored energy in the cavity. We found that the mirror system can induce asymmetric responses when energy is incident from different ports of the ring resonator, which can be used to realize nonreciprocal light transmission and on-chip integrated optical isolators.

The first passive diode was proposed by Fan *et al.* using an add-drop filter (ADF) cascaded with a notch filter, resulting in optical nonreciprocity (ONR) under a certain range of input power. In their work, the ONR response is generated initially by the ADF with asymmetric coupling quality factors to the high quality-factor silicon ring resonator, resulting in unequal stored optical energy in the cavity [11]. However, how to form an asymmetric response when the two external coupling quality factors take equal values remains unexplored. Recently, a nonconservative coupling add-drop filter (NCC-ADF) configuration is proposed in which a mirror system is supplemented to the add port [32]. When light is incident from left side of the upper waveguide, we predicted the extraordinary scattering of

---
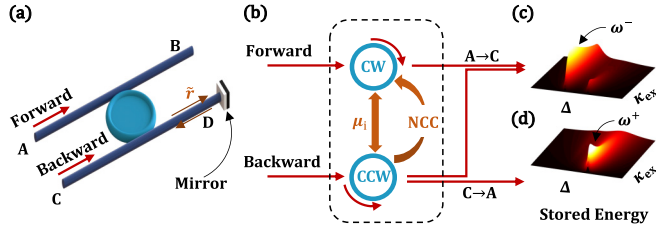
FIG. 1. (a) Schematics of an NCC-ADF. (b) Schematics of mode coupling in an NCC-ADF. (c),(d) Asymmetric stored energy in the resonator as a function of frequency detuning Δ and external coupling κ_{ex}.

the configuration in a wide parameter space [33]. Basically, the NCC-ADF is a three-port system with two degenerated modes coexisting in a single resonator. When the through port is set free, a theoretic description of mode dynamics when light is incident oppositely from the other two ports remains unrevealed. Furthermore, towards its potential application in a nonlinearity-based isolator, the role of the mirror system on the enhanced unequal stored optical energy should be determined in the first step.

In this paper, we will demonstrate that the NCC-ADF configuration can induce an asymmetric stored energy when excited at different ports. Such enhanced and tunable asymmetric response exists in both low Q-factor and high Q-factor resonators, even when the two external coupling quality factors take equal values. To confirm that, linear and nonlinear mode dynamics in the proposed configuration were effectively described and analyzed by the temporal coupled mode theory. In order to achieve integrated optical isolation, the thermal-optic nonlinearity effect was introduced to realize a low-power and broadband nonreciprocal optical transmission in the NCC-ADF configuration. Furthermore, the NCC-ADF configuration-based isolator is entirely nonmagnetic, passive, and compatible with CMOS fabrication, which is expected to be further applied in PICs.

II. THEORETICAL MODEL

A ring resonator typically supports two degenerate modes at a certain resonant frequency, which are the clockwise (CW) and counterclockwise (CCW) modes [34]. Ideally, the two modes are assumed to be uncoupled, thus the transmission spectrum is usually considered as a single peak Lorentzian. However, due to various factors such as fabrication defects [35] and deliberate design [36], coupling often occurs between two degenerate modes. Such coupling effect will remove the degeneracy of CW and CCW modes, causing a splitting of the transmission spectrum. The coupling coefficients $\mu_{\text{CW}\rightarrow\text{CCW}}$ and $\mu_{\text{CCW}\rightarrow\text{CW}}$ are employed to quantify the energy exchange of this mutual coupling effect from CW to CCW mode or from CCW to CW mode. For the conservative coupled ring resonators, the conversion coefficient of two modes is equal ($\mu_{\text{CW}\rightarrow\text{CCW}} = \mu_{\text{CCW}\rightarrow\text{CW}} = \mu_i$) and determined by internal coupling coefficient μ_i. However, the conversion efficiency of two modes is not equal ($\mu_{\text{CW}\rightarrow\text{CCW}} \neq \mu_{\text{CCW}\rightarrow\text{CW}}$) in a nonconservative coupled (NCC) ring resonator [32].

The scheme studied is shown in Fig. 1(a), where a passive ring resonator can be excited either from port A (forward direction) or port C (backward direction). An additional mirror system in port D provides a complex reflectance $\tilde{r} = r \exp(i\varphi)$ to the input signal as shown in Fig. 1(a), where r is a real constant which describes the amplitude reflection ratio and φ denotes the relative phase delay. The mirror provides a unidirectional coupling from the CCW mode to the CW mode of the resonator, as shown by the dashed box in Fig. 1(b). In a real platform, the mirror system can be implemented passively using a waveguide with an etched hole [37], waveguide Bragg grating, or another passive resonator with the same resonant frequency. Alternatively, it can also be driven actively by a semiconductor optical amplifier or another active resonator with a broad gain range [33]. Although mode exactions and light paths demonstrate different behaviors under the two incident directions as shown schematically by the red arrowed lines in Fig. 1(b), transmission should be the same, which is guaranteed by the well-known Lorentzian reciprocal theorem in any linear optical system [3]. However, stored optical energy in the linear resonator is different due to the asymmetric geometry of the system, as shown by the two parallel panels in Figs. 1(c) and 1(d). To reveal the nonreciprocal transmission physical mechanism of such phenomenon, a group of self-consistent nonlinear temporal coupled mode equations are introduced. Therefore, the asymmetric response of the NCC-ADF configuration under linear and thermal-optical nonlinearity effects can be obtained theoretically.

When light is incident from port A, i.e., the forward direction, the following nonlinear temporal coupled mode equations and input-and-output formalisms are adopted to describe the dynamics of CW and CCW modes inside the passive resonator [38]:

$$\dot{a}_{\text{CW}}^{\text{f}} = -(i\omega_{\text{c}} + \kappa/2)a_{\text{CW}}^{\text{f}} - i(\mu_i - i\tilde{r}\kappa_{\text{ex2}})a_{\text{CCW}}^{\text{f}}$$
$$- \sqrt{\kappa_{\text{ex1}}}b_{\text{in,A}}, \quad (1a)$$

$$\dot{a}_{\text{CCW}}^{\text{f}} = -(i\omega_{\text{c}} + \kappa/2)a_{\text{CCW}}^{\text{f}} - i\mu_i a_{\text{CW}}^{\text{f}}, \quad (1b)$$

$$b_{\text{out,C}}^{\text{f}} = \sqrt{\kappa_{\text{ex2}}}(a_{\text{CW}}^{\text{f}} + \tilde{r}a_{\text{CCW}}^{\text{f}}). \quad (1c)$$

The amplitudes of the CW and CCW modes are denoted by a_{CW}^{f} and $a_{\text{CCW}}^{\text{f}}$, respectively. The input signal from port A is denoted by $b_{\text{in,A}}$ and the output signal from port C is denoted by $b_{\text{out,C}}^{\text{f}}$. The cavity resonant frequency $\omega_{\text{c}} = \omega_0 + \omega_{\text{th,f}}$ is characterized by the linear resonance frequency ω_0 and the nonlinear thermal-optical effect frequency $\omega_{\text{th,f}}$ (or $\omega_{\text{th,b}}$). When the system is in a steady state, $\omega_{\text{th,f/b}} = \omega_0 \frac{\beta\tau_{\text{th}}}{n\tau_{\text{linear}}\rho C_P V}(|a_{\text{CW}}^{\text{f/b}}|^2 + |a_{\text{CCW}}^{\text{f/b}}|^2)$ was affected by the linear resonance frequency (ω_0), temperature relaxation time (τ_{th}), material refractive index (n), linear absorption coefficient ($1/\tau_{\text{linear}}$), density (ρ), material specific heat capacity (C_P), material thermal-optic coefficient (β), mode volume (V), and intracavity stored energy ($E^{\text{f/b}} = |a_{\text{CW}}^{\text{f/b}}|^2 + |a_{\text{CCW}}^{\text{f/b}}|^2$). It is assumed that external coupling coefficients κ_{ex1} and κ_{ex2} take equal values and equal to κ_{ex}, κ_i represents the intrinsic loss. As a result, the total damping rate is $\kappa = \kappa_i + \kappa_{\text{ex1}} + \kappa_{\text{ex2}}$ for either the CW or the CCW mode. Inherent modal coupling occurs between CW/CCW modes with a real coefficient μ_i, which is assumed to be identical for both directions. The nonconservative coupling coefficient can be written as $Ae^{i\phi} =$

$-i\tilde{r}\kappa_{\text{ex2}}$, which assumes that the reflected signal from port D again acts as an input power flow for the CW mode. Equations (1a) and (1b) indicate such nonconservative coupling process, which means $\mu_{\text{CCW}\to\text{CW}} = \mu_{\text{i}} - i\tilde{r}\kappa_{\text{ex2}}$ and $\mu_{\text{CW}\to\text{CCW}} = \mu_{\text{i}}$. The output signal in port C not only contains the contribution from the CW mode, but also the CCW mode which is reflected with the aid of the mirror in port D, as modeled in Eq. (1c).

When light is incident from port C, i.e., the backward direction, the incident signal can be directly coupled to a CCW mode or coupled to a CW mode with the aid of the mirror. As a result, $b_{\text{in,C}}$ will appear at both dynamics of the CW and CCW modes. The output signal in port A will have only contribution from the CCW mode. The dynamics of modes relating the input and output signals can be written as

$$\dot{a}_{\text{CW}}^{\text{b}} = -(i\omega_{\text{c}}+\kappa/2)a_{\text{CW}}^{\text{b}}-i(\mu_{\text{i}}-i\tilde{r}\kappa_{\text{ex2}})a_{\text{CCW}}^{\text{b}}-\tilde{r}\sqrt{\kappa_{\text{ex2}}}b_{\text{in,C}},$$
(2a)

$$\dot{a}_{\text{CCW}}^{\text{b}} = -(i\omega_{\text{c}} + \kappa/2)a_{\text{CCW}}^{\text{b}} - i\mu_{\text{i}}a_{\text{CW}}^{\text{b}} - \sqrt{\kappa_{\text{ex2}}}b_{\text{in,C}},$$
(2b)

$$b_{\text{out,A}}^{\text{b}} = \sqrt{\kappa_{\text{ex1}}}a_{\text{CCW}}^{\text{b}},$$
(2c)

It is worth noting that the output signal in port C has contributions not only from the CW mode, but also from reflected light by the mirror system. After employing the transformations $a_{\text{CW/CCW}}^{\text{f/b}} = A_{\text{CW/CCW}}^{\text{f/b}}e^{-i\omega t}$, $b_{\text{in,A/C}}^{\text{f/b}} = B_{\text{in,A/C}}^{\text{f/b}}e^{-i\omega t}$, and $\dot{a}_{\text{CW/CCW}}^{\text{f/b}} = -i\omega A_{\text{CW/CCW}}^{\text{f/b}}e^{-i\omega t} + \dot{A}_{\text{CW/CCW}}^{\text{f/b}}e^{-i\omega t}$ in Eqs. (1a)–(1c) and Eqs. (2a)–(2c), the transmission and intracavity stored energy can be theoretically calculated [19,39]. Here, ω is the frequency of the input laser light. If one considers all the signals in the linear system ($\omega_{\text{th,f/b}} = 0$) are with the same frequency $\omega_0 + \Delta$ in a steady status ($\dot{A}_{\text{CW/CCW}}^{\text{f/b}} = 0$), i.e., ignoring any frequency conversion process, the transmission between ports A and C can be obtained as

$$T_{\text{AC}} = T_{\text{CA}} = \left|\frac{\xi + i\mu_{\text{i}}\tilde{r}}{\xi^2 + \eta^2}\right|^2 \kappa_{\text{ex1}}\kappa_{\text{ex2}},$$
(3)

in which we have used the denotations $\xi = i\Delta - \kappa/2$ and $\eta^2 = \mu_{\text{i}}(\mu_{\text{i}} - i\tilde{r}\kappa_{\text{ex2}})$ for simplicity. Note that the frequency detuning is defined as $\Delta = \omega - \omega_{\text{c}}$, which turns to $\omega - \omega_0$ in a linear scheme. The expression in Eq. (3) is in proportion to the product $\kappa_{\text{ex1}}\kappa_{\text{ex2}}$, which indicates a higher external coupling coefficient will be preferred to achieve larger signal transmittance. If we assume that the input power is fixed at P_{in} for the forward and backward incident directions, the optical energy stored in the resonator can be calculated by the sum of contribution from both CW and CCW modes inside the resonator, which is like the definition of the term circulating power in Ref. [40]. At the stationary status, the forward and backward total stored optical energy of the NCC-ADF configuration can be denoted as

$$E^{\text{f}} = \frac{\mu_0^2 + |\xi|^2}{|\xi^2 + \eta^2|^2}\kappa_{\text{ex1}}P_{\text{in}},$$
(4a)

$$E^{\text{b}} = \frac{|i\mu_{\text{i}} + \tilde{r}(\xi + \kappa_{\text{ex2}})|^2 + |i\mu_{\text{i}}\tilde{r} + \xi|^2}{|\xi^2 + \eta^2|^2}\kappa_{\text{ex2}}P_{\text{in}}.$$
(4b)

Equations (4) indicate that the stored energy in the cavity of the NCC-ADF configuration is unequal when light is incident from the forward and backward directions, i.e., $E^{\text{f}} \neq E^{\text{b}}$, although Eq. (3) shows the same transmission when light is incident from different directions. Note that asymmetrical stored energy cannot break the Lorentz reciprocity theorem in the linear condition. Only when the NCC-ADF configuration operates in a nonlinear condition, will such energy asymmetry cause different nonlinear frequency shifts, potentially enabling optical isolation. In the case of an ideal ADF without inherent modal CW/CCW coupling or nonconservative coupling, i.e., $\mu_{\text{i}} = 0$ and $\tilde{r} = 0$, both the forward and the backward transmission spectra are a Lorentzian shape and are centered at the zero detuning with a linewidth $\delta\omega_0 = \kappa$, as can be obtained from Eq. (3). The corresponding ratio of stored energy is frequency independent and only determined by the two external coupling coefficients $R_{\text{ADF}} = \kappa_{\text{ex1}}/\kappa_{\text{ex2}}$. With $R_{\text{ADF}} \neq 1$ and a certain input power range, it is possible to design a resonator driven at an extreme status so that the redshift of the resonant wavelength $\delta\omega_{\text{NL}}$ is unequal in opposite directions. The referred extreme status has been realized by Fan *et al.* to form an optical nonreciprocity initiator [11]. Theoretically, a higher isolation ratio can be realized in a nonlinear-based nonreciprocal device with smaller $\delta\omega_0$ but larger difference in $\delta\omega_{\text{NL}}$.

III. RESULTS AND DISCUSSION

A. Linear NCC-ADF configuration with a low Q factor

We begin the discussion from a linear NCC-ADF configuration with a low Q-factor resonator ($\mu_{\text{i}} = \omega_{\text{th,f/b}} = 0$). To reveal the asymmetric response in an NCC-ADF configuration, it is assumed that parameters κ_{ex1}, κ_{ex2}, μ_{i}, and Δ are all normalized to the intrinsic decay rate κ_{i} in the following discussions for simplicity. As denoted by the schematics in Fig. 1(b), only the CW mode exists in the resonator for the forward case, while both CW and CCW modes coexist in the backward case. Although the transmission spectra share the same expression with an ideal ADF, the stored optical energy in the resonator is different for both incident directions. In the forward direction, a CW mode dominates the total energy spectrum in the resonator and shows a Lorentzian shape with a linewidth of κ. In the backward direction, a CCW mode is directly coupled from port C and should have the same trend, while the backward CW mode is generated from the uncoupled signal which is reflected from the mirror system. The corresponding optical energy spectra of the three modes can be written as

$$E_{\text{CCW}}^{\text{b}} = E_{\text{CW}}^{\text{f}} = \frac{\kappa_{\text{ex}}P_{\text{in}}}{\Delta^2 + \kappa^2/4},$$
(5a)

$$E_{\text{CW}}^{\text{b}} = r^2\left[1 - \frac{\kappa_{\text{ex}}(\kappa - \kappa_{\text{ex}})}{\Delta^2 + \kappa^2/4}\right]E_{\text{CW}}^{\text{f}}.$$
(5b)

As depicted by the schematics in Fig. 1(b), the backward CW mode makes no contribution to the transmission, but it increases the total stored optical energy. Equation (5a) shows that its contribution to the stored optical energy is in proportion to r^2 and independent of the phase delay φ. To make the point clear, we drew the optical energy spectra in Fig. 2 as κ_{ex} increases gradually from 0 to 2.

The highest stored energy is obtained at zero detuning when $\kappa_{\text{ex}} = 0.5$, as shown in Fig. 2(a), which will be referred to as a critical coupling status. The intrinsic coupling and
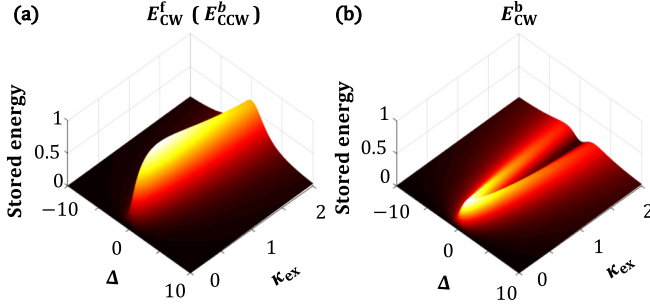
FIG. 2. Stored energies in an NCC-ADF resonator with different external coupling coefficients in the case of (a) forward CW mode or backward CCW mode and (b) backward CW mode. Other parameters are $\mu_i = 0$ and $r = 1$. Stored energies are all normalized to the maximum value at the critical coupling condition.

total external coupling contribute almost equally at this critical coupling status. When the external coupling κ_{ex} deviates from 0.5, the total stored energy in the forward direction ($E^f = E^f_{CW}$) decreases sharply in the undercoupling region ($\kappa_{ex} < 0.5$), while the total stored energy in the forward direction remains at a high level in the overcoupling region ($\kappa_{ex} > 0.5$). In the case of the backward direction, the spectrum is also a Lorentzian shape in the undercoupling region, resulting in the total stored energy in the backward direction ($E^b = E^b_{CW} + E^b_{CCW}$) being $1 + r^2$ times higher than the total stored optical energy in the forward direction. However, when κ_{ex} is comparable with or higher than 0.5, a burned hole of E^b_{CW} will emerge at zero detuning. As a result, the ratio E^b/E^f will be lowered to less than $1 + r^2$, and thus weakens the asymmetry.

B. Linear NCC-ADF configuration with a high Q factor

In the case of a linear high Q-factor resonator ($\mu_i \neq 0$, $\omega_{th,f/b} = 0$), a nonzero modal coupling must be considered [40,41]. Two supermodes with equal decay rate $\kappa/2$ coexist around frequencies $\omega^\pm = \omega_0 \pm \mu_i$; as a result, the portion of the two supermodes in a resonator will be always at the same level in a conservative coupling ADF configuration. However, in a NCC-ADF configuration, as has already been pointed out in Ref. [33], the two supermodes $\omega^\pm = \omega_0 \pm \eta_R$ will suffer from different decay rates $\kappa/2 \pm \eta_I$, with η_R and η_I denoting the real and imaginary parts of $\eta = \eta_R + i\eta_I$. Since the symmetry between the two supermodes is broken by the mirror system, an enhanced and supermode related asymmetric response in stored optical energy would be predicted.

To reveal how the symmetry-broken supermodes influence the resulted response in the NCC-ADF, we fixed the system at the critical coupling status $\kappa_{ex} = 0.5$. The inherent CW/CCW modal coupling is set at $\mu_i = 2$, which is large enough to distinguish the two supermodes. The phase delay from the mirror system is fixed at $\varphi = 0$ so that the NCC system provides a pure imaginary NCC coefficient, i.e., $\eta^2 = \mu_i(\mu_i - ir\kappa_{ex})$. The curves in Figs. 3(a) and 3(b) are the total stored energy at $r = 0$ and 1 in the forward and backward direction, respectively. The two black curves represent the case at $r = 0$, which indicates the equal contribution of the two supermodes in an ADF without a mirror system. As the
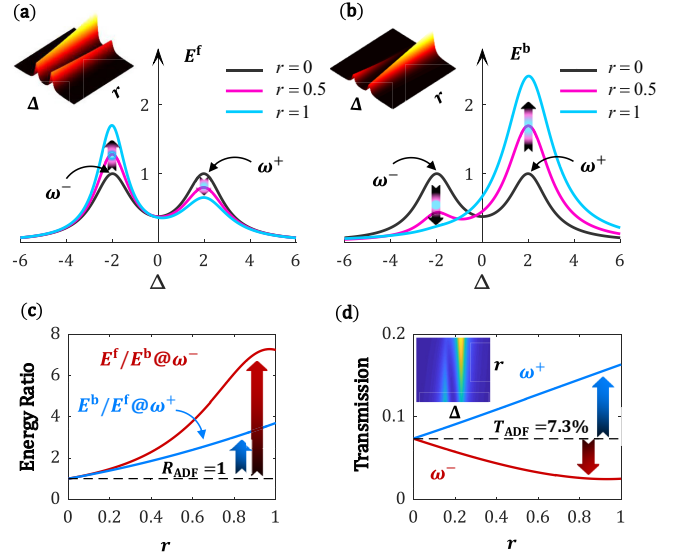
FIG. 3. Total stored energy spectra of an NCC-ADF in the case of (a) forward direction and (b) backward direction at $r = 0$ and 1, respectively. The insets in (a) and (b) show the dependence of E^f and E^b on Δ and r. (c) Ratio of stored energy when exciting the two supermodes in an NCC-ADF. (d) Transmission dependence on r for two supermodes (blue for ω^+, red for ω^-). Other parameters are $\kappa_{ex} = 0.5$, $\mu_i = 0.5$, and $\varphi = 0$. The inset in (d) shows the transmission spectra on Δ and r. The black dashed line stands for the case of an ideal ADF without a mirror system. Stored energies are all normalized to the case of an ADF without a mirror system.

reflection from the mirror r gradually increases from 0 to 1, the location of the two supermodes $\omega^\pm$ remains unchanged due to the high level of the inherent CW/CCW modal coupling coefficient μ_i. Nonetheless, the two supermodes demonstrate opposite trends. The stored optical energy of the supermode with a lower frequency ω^- is enhanced in the forward case while severely suppressed in the backward case, as shown by the arrows in Figs. 3(a) and 3(b). At the extreme status when the mirror system provides no loss or gain, i.e., $r = 1$, the stored optical energy E^f reaches 1.7 folds of its initial value, while E^b drops to a negligible value. Although the maximum ratio E^f/E^b reaches 7.3, shown by the red curve in Fig. 3(c), linear transmission drops from 7.3% to less than 1%, as shown by the red curve in Fig. 3(d). Oppositely, in the case of the supermode ω^+, stored optical energy E^f drops to 0.64 times its initial value, while E^b is increased by 2.5-fold, demonstrating a maximum ratio $E^b/E^f = 3.7$. Meanwhile, the peak transmission is increased from 7.3% to 16%, as shown by the blue curve in Fig. 3(d). The dependence of transmission spectra on r and Δ are shown in the inset of Fig. 3(d). It can be concluded that the diversity of backward and forward stored optical energy at a certain supermode can be attributed to the coherence of the CW and CCW modes inside the central resonator of the NCC-ADF configuration. The 2.5-fold enhancement in stored energy can well reduce the requirement on input power in a high-Q resonator. In a word, even when driving a high Q-factor NCC-ADF by light around ω^+ with a low input power, it is possible to obtain superior isolation based on optical nonlinearity-induced nonreciproc-
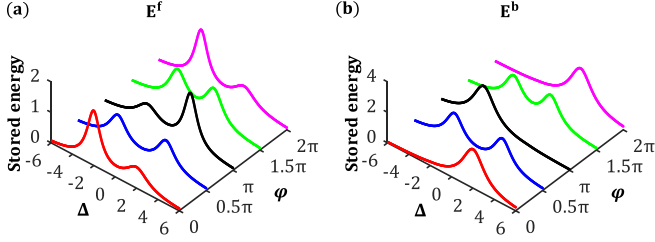
FIG. 4. Dependence of stored energy on phase delay caused by the mirror system in an NCC-ADF in the case of (a) forward direction and (b) backward direction. Stored energies are all normalized to the maximum value at the critical coupling condition. Other parameters are $\kappa_{ex} = 0.5$, $\mu_i = 2$, and $r = 1$.

FIG. 5. The nonreciprocal transmission spectrum of the thermo-optical nonlinear NCC-ADF configuration at $r = 1$, $\varphi = 0$, and $\mu_i = \kappa$ (a). The effect of μ_i/κ on the maximum NTR (MaxNTR) at different incident powers when $r = 1$ and $\varphi = 0$ (b), and the dependence of MaxNTR on r and φ when $P_{in} = 2$ mW and $\mu_i = \kappa$ (c).

ity. The NCC-ADF demonstrates an enhanced transmission and dramatically lower requirement on the input power range, thus providing the chance to break the fundamental constraint on nonlinear isolators [42].

Next, we discuss the tunability of the asymmetric response on phase delay caused by the mirror system. When the phase delay varies, the excitation of the two supermodes $\omega^{\pm}$ shows a periodic motion as shown in Figs. 4(a) and 4(b). Specifically, the switch between the two supermodes can be obtained by tuning the phase delay to 0 or π, as shown by the red and black curves in Fig. 4. When the phase delay locates at $\pi/2$ or $3\pi/2$, the additional coupling coefficient is pure real and $\eta_I = 0$. As a result, the corresponding mode-mode will only endure a slight frequency shift, as denoted by the blue and green curves in Fig. 4. Such novel asymmetric response can be interpreted by the constructive or destructive interference of light generated from the interaction of the mirror system and the ring resonator when a certain phase match is satisfied [37].

C. Nonlinear NCC-ADF configuration for passive isolators

Up to this point, the discussions above ignored the influence of the thermo-optic effect, which means that our device operated at low-power linear conditions. Next, we will delve into the nonreciprocal optical transmission of an NCC-ADF configuration under the thermal-optical nonlinearity ($\mu_i \neq 0$, $\omega_{th,f/b} \neq 0$). Silicon was used for the proposed NCC-ADF configuration, and the nonlinear coupling equations were solved with parameters $n = 3.475$, $1/\tau_{linear} = 3.9 \times 10^9 s^{-1}$, $V = 74.277 \times 10^{-18} m^3$, $\tau_{th} = 65$ns, $\rho = 2.33$g/cm^3, $C_p = 0.7$J/(g K), $\beta = 1.86 \times 10^{-4}$K^{-1}, and $Q_{ex1} = Q_{ex2} = 12\,000$. Additionally, we control the cavity in an overcoupled state ($Q_{ADF} = 120\,000$) to maximize the energy in the cavity and trigger the nonlinearity at a lower power. The nonreciprocal transmission ratio NTR $= 10 \log_{10}(T_f/T_b)$ was used to characterize the nonreciprocal properties of the structure.

As shown in Fig. 5(a), the thermo-optical nonlinear NCC-ADF configuration demonstrates significant low-power and broadband nonreciprocal transmission. This nonreciprocity is based on the splitting and shifting of the transmission spectrum, which is caused by the asymmetric energy stored in the cavity during the increase of forward and backward incident power. The slopes of peak change were quantified by the colored dotted lines in Fig. 5(a). As the input power increases,
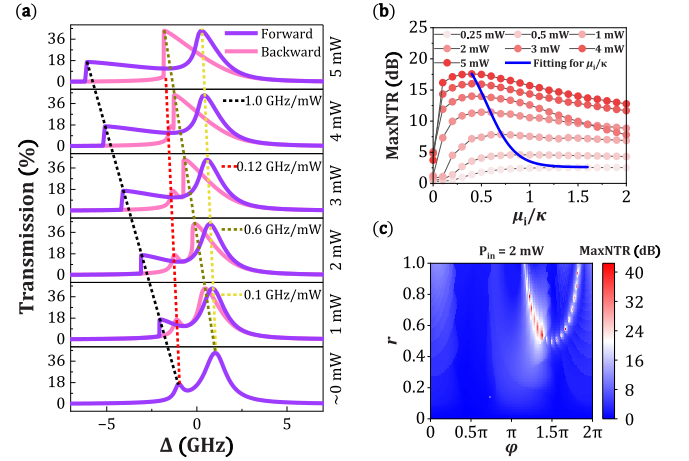
the black dotted and green dotted lines exhibit significant shifts. Especially when $E^b_{CW} = E^b_{CCW}$, the splitting of backward incidence will disappear. The fitting of μ_i/κ in Fig. 5(b) provides the optimal μ_i values for achieving MaxNTR at each input power when $r = 1$ and $\varphi = 0$, indicating that the value of μ_i is crucial for achieving better optical isolation at different input powers. Specifically, the splitting between two supermodes in the system is different when μ_i takes different values relative to κ, which will greatly affect the stored energy in the cavity [33]. When $\mu_i = 0$, the ability of the mirror system to enhance asymmetric stored energy in the cavity is limited, thereby requiring higher power to achieve efficient optical isolation. A larger μ_i does not necessarily imply better optical isolation, which may also hinder on-chip optical isolation. Recently, a scheme to control the mode splitting in high-Q microcavities makes it possible to dynamically change the μ_0 value to achieve a larger nonreciprocal ratio [43]. Furthermore, a scan of the MaxNTR that parameters r and φ can generate at $P_{in} = 2$ mW and $\mu_i = \kappa$ was conducted, as shown in Fig. 5(c). It is observed that when φ is at $0(2\pi)$ and π, the MaxNTR reaches its peak, while valleys appear when φ equals 0.5π and 1.5π. As explained in Fig. 4, when $\varphi = 0$ or π, the maximum energy asymmetry between forward and backward incidence will result in significant nonreciprocal light transmission. Conversely, when $\varphi = 0.5\pi$ or 1.5π, the energy storage in the cavity is nearly equal, and nonreciprocal transmission does not occur even under the thermo-optic nonlinearity. Anyway, the proposed NCC-ADF configuration can significantly enhance the energy in the cavity and realizes the tunable nonreciprocal optical transmission with low power and bandwidth under the thermo-optical nonlinearity. In addition, the NCC-ADF configuration is expected to be combined with Kerr nonlinearity, with the help of cascaded microring structures to achieve a greater optical isolation through the interaction of Kerr nonlinearity and thermo-optical nonlinearity.

IV. CONCLUSIONS

In conclusion, we have introduced a temporal coupling mode theory to reveal the linear and nonlinear mode dynamics in an NCC-ADF configuration. The NCC-ADF configuration has a low requirement for the cavity quality factors, demonstrates asymmetric response even in low Q-factor resonators with two equal external coupling quality factors. Particularly, the proposed configuration can enhance the stored energy in a high Q-factor resonator by 2.5-fold in the backward direction, reducing the high-power requirement of achieving the nonlinear effects. Furthermore, the proposed configuration can be used to realize nonreciprocal transmission under thermo-optical nonlinearity, which compensates for the low power, bandwidth, and tunable requirements of a passive nonlinear isolator. Such asymmetric response might find potential application in on-chip optical isolators as well as other applications based on add-drop configurations.

[1] T. Komljenovic, D. N. Huang, P. Pintus, M. A. Tran, M. L. Davenport, and J. E. Bowers, Photonic integrated circuits using heterogeneous integration on silicon, Proc. IEEE **106**, 2246 (2018).

[2] L. Feng, M. Ayache, J. Huang, Y. L. Xu, M. H. Lu, Y. F. Chen, Y. Fainman, and A. Scherer, Nonreciprocal light propagation in a silicon photonic circuit, Science **333**, 729 (2011).

[3] C. Caloz, A. Alù, S. Tretyakov, D. Sounas, K. Achouri, and Z. L. Deck-Léger, Electromagnetic nonreciprocity, Phys. Rev. Appl. **10**, 047001 (2018).

[4] C. J. Firby and A. Y. Elezzabi, High-speed nonreciprocal magnetoplasmonic waveguide phase shifter, Optica **2**, 598 (2015).

[5] K. Srinivasan and B. J. H. Stadler, Magneto-optical materials and designs for integrated TE- and TM-mode planar waveguide isolators: A review, Opt. Mater. Express **8**, 3307 (2018).

[6] L. Bi, J. Hu, P. Jiang, D. H. Kim, G. F. Dionne, L. C. Kimerling, and C. A. Ross, On-chip optical isolation in monolithically integrated non-reciprocal optical resonators, Nat. Photonics **5**, 758 (2011).

[7] H. Lira, Z. Yu, S. Fan, and M. Lipson, Electrically driven nonreciprocity induced by interband photonic transition on a silicon chip, Phys. Rev. Lett. **109**, 033901 (2012).

[8] J. Kim, M. C. Kuzyk, K. Han, H. Wang, and G. Bahl, Nonreciprocal Brillouin scattering induced transparency, Nat. Phys. **11**, 275 (2015).

[9] H. Tian, J. Liu, A. Siddharth, R. N. Wang, T. Blésin, J. He, T. J. Kippenberg, and S. A. Bhave, Magnetic-free silicon nitride integrated optical isolator, Nat. Photonics **15**, 828 (2021).

[10] M. Cotrufo, S. A. Mann, H. Moussa, and A. Alu, Nonlinearity-induced nonreciprocity—Part I, IEEE Trans. Microwave Theory Tech. **69**, 3569 (2021).

[11] L. Fan, J. Wang, L. T. Varghese, H. Shen, B. Niu, Y. Xuan, A. M. Weiner, and M. Qi, An all-silicon passive optical diode, Science **335**, 447 (2012).

[12] K. Y. Yang, J. Skarda, M. Cotrufo, A. Dutt, G. H. Ahn, M. Sawaby, D. Vercruysse, A. Arbabian, S. H. Fan, A. Alu, and J. Vuckovic, Inverse-designed non-reciprocal pulse router for chip-based LiDAR, Nat. Photonics **14**, 369 (2020).

[13] A. D. White, G. H. Ahn, K. V. Gasse, K. Y. Yang, L. Chang, J. E. Bowers, and J. Vuckovic, Integrated passive nonlinear optical isolators, Nat. Photonics **17**, 143 (2023).

[14] Y. Shi, Z. F. Yu, and S. H. Fan, Limitations of nonlinear optical isolators due to dynamic reciprocity, Nat. Photonics **9**, 388 (2015).

[15] Q. T. Cao, H. Wang, C. H. Dong, H. Jing, R. S. Liu, X. Chen, L. Ge, Q. Gong, and Y. F. Xiao, Experimental demonstration of spontaneous chirality in a nonlinear microresonator, Phys. Rev. Lett. **118**, 033901 (2017).

[16] J. Qie, C. Wang, and L. Yang, Chirality induced nonreciprocity in a nonlinear optical microresonator, Laser Photonics Rev. **17**, 2200717 (2023).

[17] Y. Q. Hu, Y. H. Qi, Y. You, S. C. Zhang, G. W. Lin, X. L. Li, J. B. Gong, S. Q. Gong, and Y. P. Niu, Passive nonlinear optical isolators bypassing dynamic reciprocity, Phys. Rev. Appl. **16**, 014046 (2021).

[18] L. Chang, X. S. Jiang, S. Y. Hua, C. Yang, J. M. Wen, L. Jiang, G. Y. Li, G. Z. Wang, and M. Xiao, Parity-time symmetry and variable optical isolation in active-passive-coupled microresonators, Nat. Photonics **8**, 524 (2014).

[19] B. Peng, S. K. Ozdemir, F. C. Lei, F. Monifi, M. Gianfreda, G. L. Long, S. H. Fan, F. Nori, C. M. Bender, and L. Yang, Parity-time-symmetric whispering-gallery microcavities, Nat. Phys. **10**, 394 (2014).

[20] X. Huang, C. Lu, C. Liang, H. Tao, and Y. C. Liu, Loss-induced nonreciprocity, Light Sci. Appl. **10**, 30 (2021).

[21] L. Wu, Y. Dong, J. Zhao, D. Ma, W. Huang, Y. Zhang, Y. Wang, X. Jiang, Y. Xiang, J. Li, Y. Feng, J. Xu, and H. Zhang, Kerr nonlinearity in 2D graphdiyne for passive photonic diodes, Adv. Mater. **31**, 1807981 (2019).

[22] D. W. Wang, H. T. Zhou, M. J. Guo, J. X. Zhang, J. Evers, and S. Y. Zhu, Optical diode made from a moving photonic crystal, Phys. Rev. Lett. **110**, 093901 (2013).

[23] S. Maayani, R. Dahan, Y. Kligerman, E. Moses, A. U. Hassan, H. Jing, F. Nori, D. N. Christodoulides, and T. Carmon, Flying couplers above spinning resonators generate irreversible refraction, Nature (London) **558**, 569 (2018).

[24] R. Huang, A. Miranowicz, J.-Q. Liao, F. Nori, and H. Jing, Nonreciprocal photon blockade, Phys. Rev. Lett. **121**, 153601 (2018).

[25] W. Mao, Z. Fu, Y. Li, F. Li, and L. Yang, Exceptional–point–enhanced phase sensing, Sci. Adv. **10**, eadl5037 (2024).

[26] Q. Zhong, J. Ren, M. Khajavikhan, D. N. Christodoulides, Ş. K. Özdemir, and R. El-Ganainy, Sensing with exceptional surfaces

in order to combine sensitivity with robustness, Phys. Rev. Lett. **122**, 153902 (2019).

[27] A. Hashemi, K. Busch, D. N. Christodoulides, S. K. Ozdemir, and R. El-Ganainy, Linear response theory of open systems with exceptional points, Nat. Commun. **13**, 3281 (2022).

[28] Q. Zhong, J. Kou, Ş. K. Özdemir, and R. El-Ganainy, Hierarchical construction of higher-order exceptional points, Phys. Rev. Lett. **125**, 203602 (2020).

[29] S. Soleymani, Q. Zhong, M. Mokim, S. Rotter, R. El-Ganainy, and Ş. K. Özdemir, Chiral and degenerate perfect absorption on exceptional surfaces, Nat. Commun. **13**, 599 (2022).

[30] Q. Zhong, S. K. Ozdemir, A. Eisfeld, A. Metelmann, and R. El-Ganainy, Exceptional-point-based optical amplifiers, Phys. Rev. Appl. **13**, 014070 (2020).

[31] K. Liao, Y. Zhong, Z. Du, G. Liu, C. Li, X. Wu, C. Deng, C. Lu, X. Wang, C. T. Chan, Q. Song, S. Wang, X. Liu, X. Hu, and Q. Gong, On-chip integrated exceptional surface microlaser, Sci. Adv. **9**, eadf3470 (2023).

[32] H. Du, X. Zhang, C. G. Littlejohns, D. T. Tran, X. Yan, M. Banakar, C. Wei, D. J. Thomson, and G. T. Reed, Nonconservative coupling in a passive silicon microring resonator, Phys. Rev. Lett. **124**, 013606 (2020).

[33] K. Zhou, Q. Liu, J. Lin, P. Jin, Q. Yang, and S. Liu, Extraordinary transmission in an add-drop filter configuration driven by nonconservative coupling, Opt. Lett. **46**, 5284 (2021).

[34] M.-Y. Ye, M.-X. Shen, and X.-M. Lin, Ringing phenomenon based measurement of weak mode-coupling strength in an optical microresonator, Sci. Rep. **7**, 17412 (2017).

[35] A. Li, T. Van Vaerenbergh, P. De Heyn, P. Bienstman, and W. Bogaerts, Backscattering in silicon microring resonators: A quantitative analysis, Laser Photonics Rev. **10**, 420 (2016).

[36] H. Lee, A. Kecebas, F. Wang, L. Chang, S. K. Özdemir, and T. Gu, Chiral exceptional point and coherent suppression of backscattering in silicon microring with low loss Mie scatterer, eLight **3**, 20 (2023).

[37] J. Wang, J. Lin, P. Jin, S. Liu, and K. Zhou, Fano resonance in a microring resonator with a micro-reflective unit, Opt. Express **31**, 31587 (2023).

[38] B. E. Little, S. T. Chu, H. A. Haus, J. Foresi, and J. P. Laine, Microring resonator channel dropping filters, J. Lightwave Technol. **15**, 998 (1997).

[39] Y.-F. Xiao, Ş. K. Özdemir, V. Gaddam, C.-H. Dong, N. Imoto, and L. Yang, Quantum nondemolition measurement of photon number via optical Kerr effect in an ultra-high-Q microtoroid cavity, Opt. Express **16**, 21462 (2008).

[40] T. J. Kippenberg, S. M. Spillane, and K. J. Vahala, Modal coupling in traveling-wave resonators, Opt. Lett. **27**, 1669 (2002).

[41] M. L. Gorodetsky, A. D. Pryamikov, and V. S. Ilchenko, Rayleigh scattering in high-Q microspheres, J. Opt. Soc. Am. B **17**, 1051 (2000).

[42] D. L. Sounas and A. Alù, Fundamental bounds on the operation of Fano nonlinear isolators, Phys. Rev. B **97**, 115431 (2018).

[43] Z. Tao, B. Shen, W. Li, L. Xing, H. Wang, Y. Wu, Y. Tao, Y. Zhou, Y. He, C. Peng, H. Shu, and X. Wang, Versatile photonic molecule switch in multimode microresonators, Light Sci. Appl. **13**, 51 (2024).